Chapter 5

A quasi solid state dye sensitized solar cell based on gelatin/multiwalled carbon nanotube gel electrolyte and zinc oxide (ZnO) nanorod photoanode

GRAPHICAL ABSTRACT

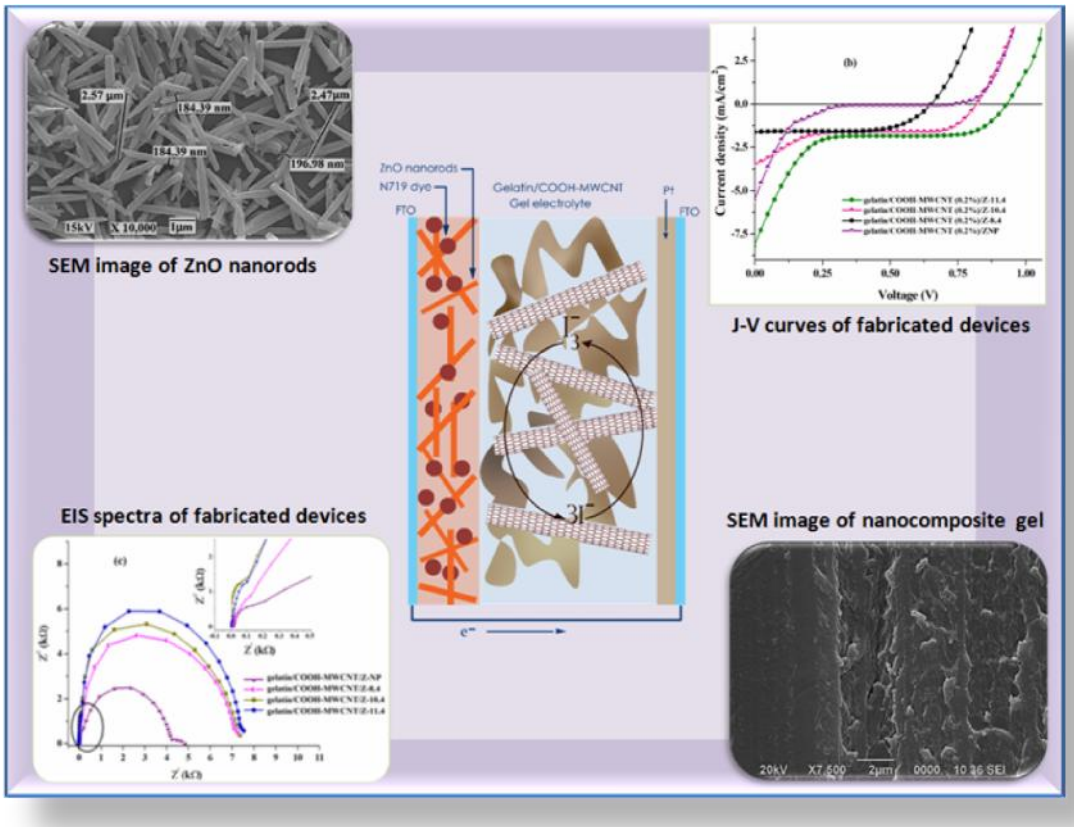

The high aspect ratio ZnO nanorods are very effective as the photoanode in quasi solid state DSSCs as they provide rapid charge transport through the channels of the nanorods thus reducing the charge recombination in the photoanode

5.1 Introduction

Most recently, DSSCs have attracted a considerable interest due to its ease of fabrication, low cost, high efficiency and light weight product as compared to conventional solid state solar cells.[1] A conventional DSSC comprises of mainly three components: a photoanode, a catalytic electrode (counter electrode) and an electrolyte with I^-/I_3^- redox couple. In a typical TiO_2 based DSSC, the photoanode and the redox couple I^-/I_3^- exhibit a good electron transport and collection imparting high efficiency to the cells (~11%).[2, 3] An increased light harvesting ability as well as an enhanced photocurrent requires a higher surface area frame work and low charge recombination. To achieve this obligation, various architectures were synthesized; for instance, ZnO nanorods, ZnO platelets, porous TiO_2 etc.[4-6] Among other morphologies, one dimensional nanostructures, such as nanorods and nanowires are superior as the photoanode creates a direct transport of charge to the anode. This increases the diffusion rate and simultaneously decreases the recombination rate resulting in higher efficiency of the device.[7] On the contrary, in a conventional DSSC the electrons diffuse to the anode by bouncing number of times between the nanoparticles and with each bounce it has the tendency to recombine with the electrolyte. Consequently, the recombination resistance becomes comparable with the transport resistance, thus impeding the efficiency of the device.

S. Sharma, M. Khannam, S.K Dolui, *J. Mater. Sci. Mater. Electron.* (Just accepted-DOI: 10.1007/s10854-016-4777-x)

One dimensional ZnO nanostructures can be considered as an alternative to TiO_2-photoanodes in DSSCs, because of the ease of deposition of one dimensional ZnO nanostructures on conducting FTO/ITO substrates.[8] ZnO has almost similar energy band gap and better electron transport property compared to TiO_2.[7] Till now diverse approaches have been deployed to use one dimensional ZnO nanostructures, which show potent application of the nanostructure in the field of DSSCs. The application of ZnO nanowire composite with ZnO nanoparticles by chemical bath deposition methods in DSSCs was investigated with maximum PCE of 1.27-2.37%.[8] ZnO nanowires with a maximum PCE of 0.66%, deposited electrochemically and post-treated by hydrothermal method can be considered as an efficient photoanode in DSSCs.[9] The electron transport mechanism in DSSCs was also investigated for ZnO nanorods films deposited by metal organic chemical vapour deposition (MOCVD).[10] DSSCs with vertically aligned, single-crystalline, MOCVD-grown ZnO nanorod electrodes lead much faster electron transport than mesoporous ZnO nanoparticle electrodes.[10] The electron transport is 10 to 100 times faster in photoanodes composed of ZnO nanorods compared to standard photoanodes assembled with colloidal nanoparticles.[11] ZnO nanorods grown on indium doped ZnO film as photoanode showed PCE of 0.56%.[12] Photovoltaic cells fabricated from ZnO/TiO_2 hybrid photoanode showed a maximum PCE of 2.94%.[13] But the method requires great care during the $TiCl_4$ treatment of the hybrid photoanode. The dissolution of the ZnO nanostructures with titanium tetrachloride ($TiCl_4$) was its major drawback. The DSSCs fabricated with 3.2 μm ZnO nanotip array exhibited a PCE of 0.55% under 1 sun irradiance.[14] Recently, a number literatures are found which also show the potentiality of one-dimensional ZnO nanostructures as a photoanode in DSSCs.[15-19]

In recent times, polymer gel electrolyte offers a wide field of research due to its prevention towards solvent leakage and evaporation inside the cell. Still the effect of such electrolytes in ZnO photoanode based DSSCs is yet to study. Considering these aspects, a series of quasi solid state DSSCs have been fabricated by using different aspect ratio ZnO nanorods as photoanodes. An attempt has been made to replace the conventional liquid electrolyte with a gelatin/MWCNT gel electrolyte. In a polymer gel electrolyte the liquid electrolyte is entrapped into the gel matrix that prevents leakage and evaporation of the solvent.[20] Ions present in the electrolyte can move

easily in the solution phase inside the gel providing better ionic conductivity. Gelatin is one of the most suitable polymers for solar cells, because of its excellent film forming ability under simple experimental conditions.[21, 22] MWCNT provides large surface area for charge transport inside the gel electrolyte that offers better photovoltaic performance to the cell.[23]

5.2 Experimental

5.2.1 Reagents

The chemicals gelatin (from porcin skin), glutaraldehyde, multiwalled carbon nanotubes (MWCNT), lithium iodide (LiI), tert-bytyl pyridine (TBP), 1-methyl-3-propyl imidazolium iodide (MPII), iodine (I_2), Cis-bis(isothiocyanato)bis(2,2′-bipyridyl-4,4′-dicarboxylato) ruthenium (II) bis-tetrabutylammonium (N-719) and fluorine doped tin oxide (FTO) coated glasses (Sheet resistance: 15Ω/sq) were purchased from Sigma Aldrich. Zinc acetate ($Zn(CH_3COO)_2$), sodium hydroxide (NaOH), cetyl trimethyl ammonium bromide (CTAB), nitric acid, acetonitrile, ethanol and N-methyl-2-pyrrolidone (NMP) were purchased from Merck.

5.2.2 Functionalization of multiwalled carbon nanotube (MWCNT)

MWCNT was functionalized with carboxyl group by a method reported earlier.[24] Firstly, MWCNTs were added into a round bottomed flask containing concentrated nitric acid and allowed to reflux for 12 h. Then the functionalized MWCNTs (COOH-MWCNTs) were filtered, washed with distilled water and finally dried at 100 °C in an oven. This purification step added oxygenated functionalities onto the nanotube surface.

5.2.3 Synthesis of gelatin/COOH-MWCNT gel electrolyte

One step chemical method was utilized to synthesize gelatin gel with and without COOH-MWCNT.[25] In particular a 10% gelatin solution was added to COOH-MWCNT (0.025%, 0.05%, 0.1% and 0.2%) and subsequently stirred for 2 h. The mixture was further cured at 60-70 °C after addition of a specific amount of cross-linker (1.5 mL), glutaraldehyde. Curing turns the mixture into a desired gel within a

few minutes. In order to remove the unwanted cross-linker from the surface of the gel, the synthesized product was washed thoroughly with double distilled water for several times, followed by drying at 50 °C.

The gel electrolyte was prepared by soaking a required amount of the gel film (0.5 g) in a liquid electrolyte solution comprising of 0.1 M LiI, 0.6 M I_2, 0.5 M TBP and 0.05 M MPII in a mixed solvent of NMP and acetonitrile in the ratio of 2:8. The film was soaked for 96 h to reach absorption saturation.

5.2.4 Synthesis of ZnO nanorods

Three sets of ZnO nanorods were synthesized by one pot hydrothermal method.[26] Firstly, a solution was prepared by adding $Zn(CH_3COO)_2$ and CTAB in distilled water at a fixed molar ratio of 1:1.5. To this solution, 0.6 M NaOH (aq) solution was added dropwise, by maintaining the pH of the solution in the range 8.4-11.4. Then the mixture was transferred to a Teflon-lined autoclave and kept into a hot air oven at 100 °C for 16 h. Then the autoclave was allowed to cool. Products were filtered, washed thoroughly with distilled water and ethanol to remove the un-reacted surfactant followed by drying in vacuum at 50 °C. The synthesized ZnO nanorods were denoted as Z-8.4, Z-10.4 and Z-11.4 respectively, where the number denotes the pH of the medium.

5.2.5 Preparation of photoanodes

Cleaning of FTO coated glass slides was done by an ultrasonication. The sequence wise use of the detergent solution, distilled water, acetone and ethanol, cause proper cleaning of the glasses and finally dried under N_2 atmosphere. A paste of pre-synthesized ZnO nanorods [Z-8.4, Z-10.4 and Z-11.4] with ethanol was deposited onto FTO coated glass by doctor blade technique. Films were sintered at 150 °C for 1h to retain the texture. The fabricated photoanodes were immersed into dye solution for 24 h to achieve the adsorption saturation. For comparison, a set of commercially available ZnO nanorod films were sintered at 150 °C for 1h followed by adsorption of dye solution for sensitization of the photoanodes.

5.2.6 Fabrication of DSSCs

Sensitization of photoanodes was done by immersing the ZnO films in a 0.3 mM N719 dye solution in acetonitrile and ethanol with a volume ratio of 1:1 for 24 h. After the complete adsorption of the dye, the photoanodes were washed with ethanol and dried in air. The pre-synthesized gelatin/COOH-MWCNT gel electrolyte was spread evenly on the dye adsorbed photoanodes. One platinum coated FTO glass slide was placed over the gel electrolyte which can act as the counter electrode. A number of devices were fabricated either by changing the concentration of COOH-MWCNT in the electrolyte or by using different aspect ratio ZnO nanorods in the photoanode. All the devices were kept at 70 °C for 10 min prior to the photovoltaic measurements to ensure the penetration of the electrolyte into the dye sensitized photoanodes.

5.3 Instruments and methods

5.3.1 Transmission electron microscopy (TEM)

Transmission electron microscopy (TEM) image of functionalized MWCNT was revealed by JEM 2100 transmission electron microscope (TEM) with an acceleration voltage of 100-300 kV.

5.3.2 Scanning electron microscopy (SEM)

The surface morphology of synthesized ZnO nanorods and gelatin/COOH-MWCNT nanocomposite gel was investigated by JSM-6390LV, (JEOL, Japan) scanning electron microscope (SEM) at an accelerating voltage of 5-15 kV. The surface of the sample was Pt coated before observation in SEM.

5.3.3 X-ray diffractometer (XRD)

Powder X-ray diffraction (XRD) data of the synthesized ZnO nanorods was revealed by Rigaku X-ray diffractometer (Miniflex, UK) under CuK_{α} (λ= 0.154nm). Spectra were taken under 30 kV of X-ray radiation and 15 mA current with a scanning rate of $2° \text{ min}^{-1}$ at a 2θ ranging from 10° to 80°.

5.3.4 Fourier transform infrared spectrometer (FT-IR)

Fourier transform infrared (FT-IR) analysis of the synthesized nanocomposite gel was studied by FT-IR Nicolet, (Impact 410) spectrophotometer (USA). A required amount of samples was grounded and mixed properly with dried KBr followed by a compression moulding under vacuum to prepare the pellets for analysis. The spectra were recorded in transmission mode in the range of 4000-400 cm^{-1} with a nominal resolution of 4 cm^{-1}.

5.3.5 Ultraviolet-visible spectroscopy (UV-visible)

Ultraviolet-visible spectroscopy (UV-vis) study of the solid nanocomposite samples was carried out in a Shimadzu UV-2550 ultraviolet-visible spectrophotometer at a wavelength ranges from 200 to 800 nm.

5.3.6 Electrochemical impedance spectroscopy (EIS)

The electrochemical impedance spectroscopy (EIS) analysis of the fabricated DSSCs was performed on SP-150 Potentiostat Galvanostat electrochemical impedance workstation. Analysis was done at a constant temperature of 25 °C with ac signal amplitude ranges from 90 to 264 V with a frequency range of 4 Hz-100 kHz.

5.3.7 Thermogravimetric analysis (TGA)

The thermogravimetric analysis (TGA) was carried out in a Shimazdu TGA 50 thermal analyzer with a heating rate of 10 °C min^{-1} under inert atmosphere of nitrogen and a temperature range of 25-600 °C (flow rate: 30 mL min^{-1}).

5.3.8 Differential scanning calorimetry (DSC)

The glass-transition temperature of the synthesized nanocomposite gel was studied by using a Shimadzu DSC-60 differential scanning calorimeter (DSC) under the inert atmosphere of nitrogen. The analysis was run at a scanning speed of 10 °C min^{-1} and a temperature ranges from 25 to 250 °C.

5.3.9 Photovoltaic test

The photovoltaic characteristic of the fabricated DSSCs was revealed under

llumination of a 100 mW/cm^2 solar simulator in ambient atmosphere and photovoltaic parameters were calculated using the following equations:[27]

$$\text{Fill factor, FF} = \frac{J_{max}.V_{max}}{J_{sc}.V_{oc}} \qquad \text{Eqn. 5.1}$$

$$\text{Maximum power, } P_{max} = J_{max}.V_{max} = J_{sc}.V_{oc}.FF \qquad \text{Eqn. 5.2}$$

$$\eta = \frac{P_{max}}{P_{in}} = \frac{J_{sc}.V_{oc}.FF}{P_{in}} \qquad \text{Eqn. 5.3}$$

Where, J_{max} and V_{max} are the current density and voltage respectively at the maximum power point of the photocurrent density versus voltage plot. J_{sc} and V_{oc} are the short circuit current density and open circuit voltage respectively. FF is the fill factor. P_{in} is the intensity of the white light and η is the PCE of the device.

5.4 Results and discussion

5.4.1 Morphology (TEM, SEM)

Morphology of COOH-MWCNTs was studied by TEM analysis [Fig. 5.1]. The surface of MWCNTs becomes rough due to functionalization and length is reduced. This improved morphology facilitates the dispersion of the MWCNTs into the polymer matrix.[28]

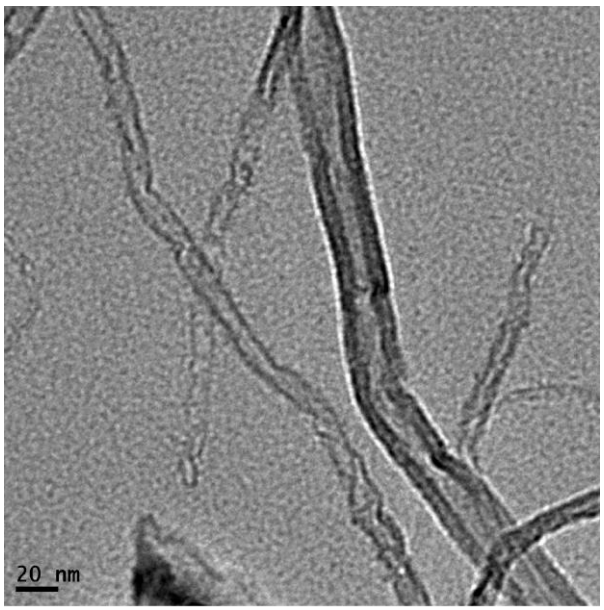

Fig. 5.1 TEM image of COOH-MWCNT

Fig. 5.2 (a) & (b) depict the respective cross-sectional SEM images of the gel COOH-MWCNT. Fig. 5.2 (a) depicts a uniform surface morphology of the pristine gelatin. However, for polymer nanocomposite gel [Fig. 5.2 (b)], surface becomes homogeneous with the addition of carbon nanotubes into the polymer matrix. The presence of COOH-MWCNT into the gelatin matrix was confirmed by EDX spectra [Fig. 5.2 (c) & (d)]. By comparing the EDX spectra, it has been observed that O and C atoms are present in all the samples, but in the nanocomposite weight % of the same is increased due to the presence of COOH-MWCNT.

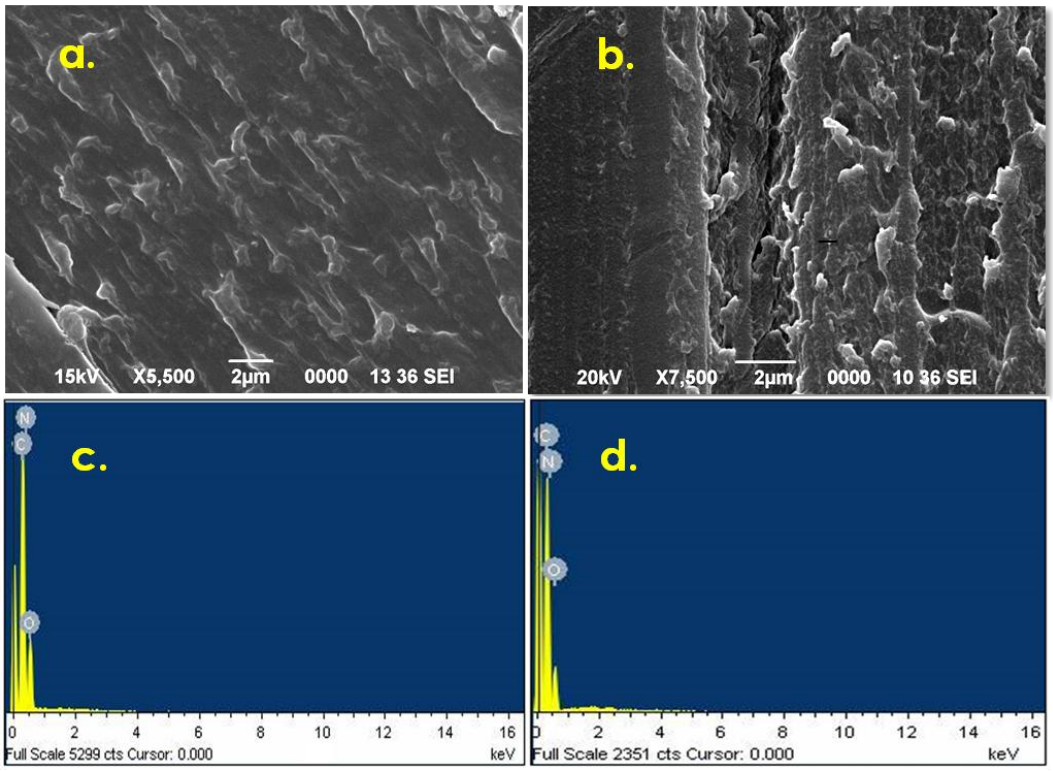

Fig. 5.2 SEM images of (a) gelatin, (b) gelatin/COOH-MWCNT, EDX spectra of (c) gelatin, (d) gelatin/COOH-MWCNT

Morphology of synthesized ZnO nanorods was analysed through SEM micrographs [Fig. 5.3]. The micrographs show the formation of rod-shaped ZnO nanocrystals with a diameter in the range 155-188 nm at pH ranging from 8.4 to 11.4. The pH dependent growth of nanorods can be explained by the fact that with increase in pH from 8.4 to 10.4, the concentrations of both Zn^{2+} and OH^- become equally significant that allows particle to grow in both lateral and longitudinal directions. Consequently, both diameter and length of the nanorods increases with increase in pH. At pH above 10.4, the excess OH^- concentration dominates that of Zn^{2+} and subsequently particle growth

is restricted except one particular direction. That allows significant increase in aspect ratio of the nanorods. For instance, the aspect ratios of nanorod are 8 and 20 when pHs of the reaction media are 8.4 and 11.4 respectively. EDX spectrum of ZnO nanorods [Z-11.4] shows the presence of both Zn and O atoms in the nanostructure that confirms the formation of ZnO nanorods [Fig. 5.3 (d)].

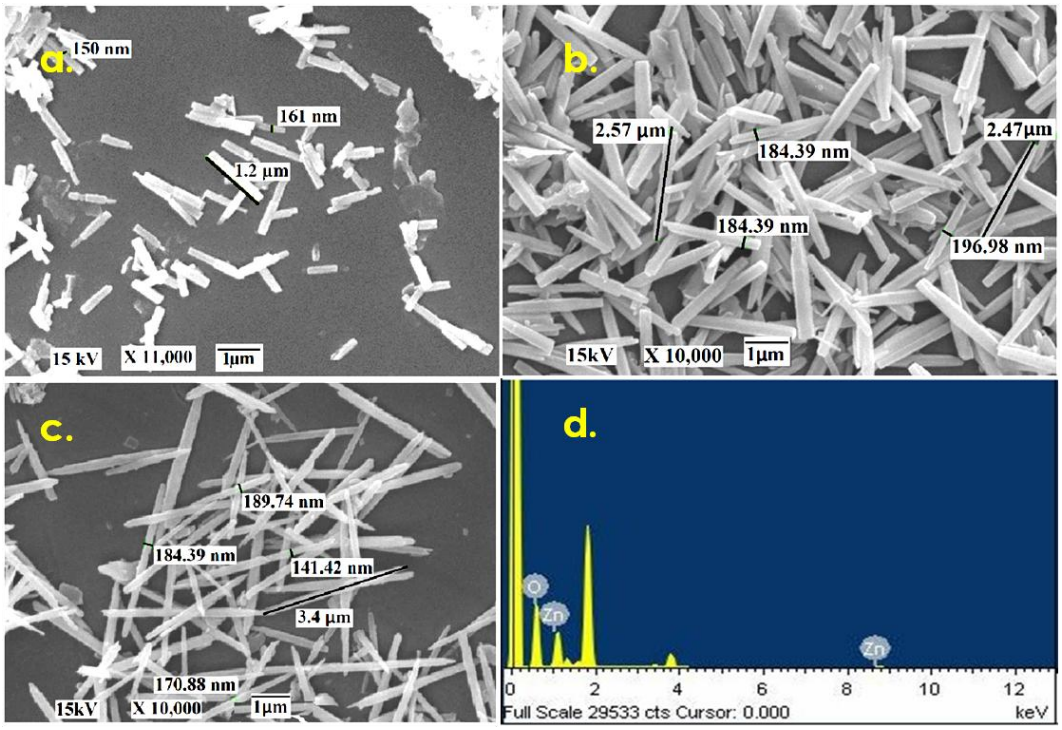

Fig. 5.3 SEM micrographs of (a) Z-8.4, (b) Z-10.4, (c) Z-11.4, (d) EDX spectrum of Z-11. *The number denotes the pH

5.4.2 Structural analysis (XRD, FT-IR)

XRD pattern [Fig. 5.4] shows the formation of highly crystalline ZnO nanorods [Z-8.4, Z-10.4 and Z-11.4]. The pattern reveals the formation of hexagonal ZnO nanocrystals with preferred crystallographic orientation along (101) (JCPDS card no. 75-0576).[29] Under hydrothermal condition, the polar planes of ZnO nanocrystals preferentially grow along (001) direction rather than other directions in order to minimize the energy, thus leading to the growth of nanorods, as confirmed by XRD analysis.[30] Due to the preferential orientation along one particular axis makes the (101) diffraction peak of ZnO nanorods stronger and narrower than the other peaks.[31] The average crystallite size of ZnO nanorods were calculated by Scherrer equation (Eqn. 5.4) using (101) plane

$$D = 0.89\ (\lambda/\beta\cos\theta) \qquad \text{Eqn. 5.4}$$

where, λ: wavelength (CuKα) = 0.154nm, β: Full width at half-maxima (FWHM) of ZnO (101) line, θ: the diffraction angle. It is observed that the average crystallite size increases from 27 to 35 nm with increase in pH from 8.4 to 11.4. The preferential particle growth along (001) at higher pH of the medium causes this increase in crystallite diameter and simultaneous increase in length of the nanorods.

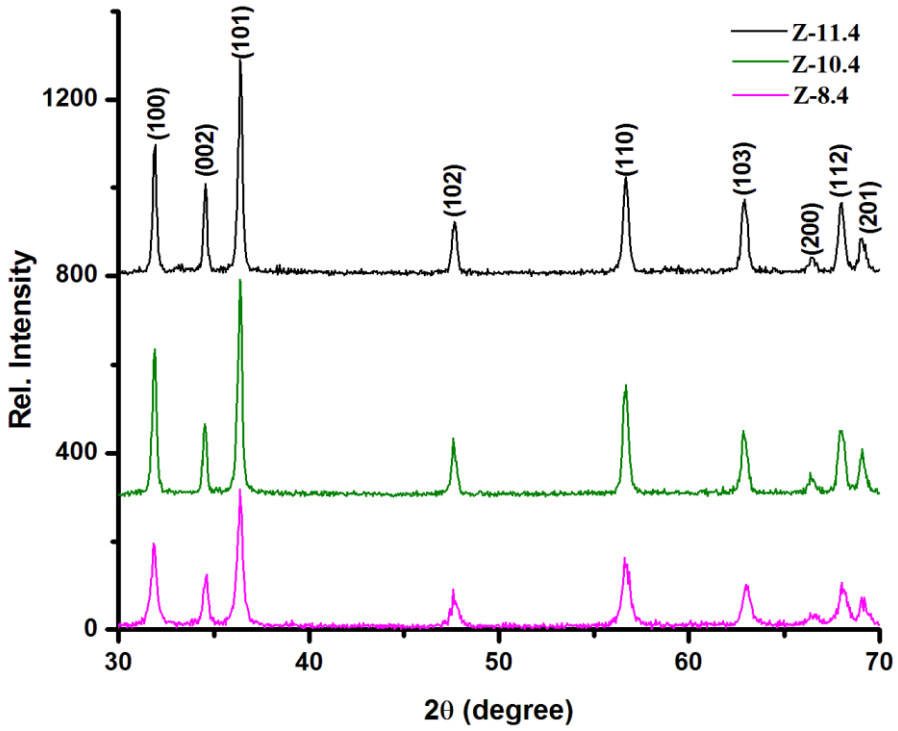

Fig. 5.4 XRD patterns of synthesized ZnO nanorods. *The number denotes the pH

The structural characteristics of the synthesized nanocomposite gel are investigated by FT-IR [Fig. 5.5] and summary of the results are shown in Table 5.1. In the spectra of COOH-MWCNT, all the characteristic peaks are found at around 3415 cm^{-1}, 1707 cm^{-1}, 1631 cm^{-1}, 1389 cm^{-1} and 1027 cm^{-1} which are due to O-H stretching, C=O stretching, C=C stretching, C-O stretching and O-H bending respectively.[32] This confirms the attachment of -COOH group on the MWCNTs. In the spectra of the gelatin, a characteristic peak is observed at 1384 cm^{-1} which is due to the presence of the aldimine linkage.[33, 34] Aldimine linkage is formed during cross-linking of the polymer when the aldehyde group (-CHO) of glutaraldehyde reacts with the amino

group (-NH_2) of the lysine residue of the proteins.[33] All the characteristic peaks are found in the nanocomposites with a remarkable shift towards higher wave number.

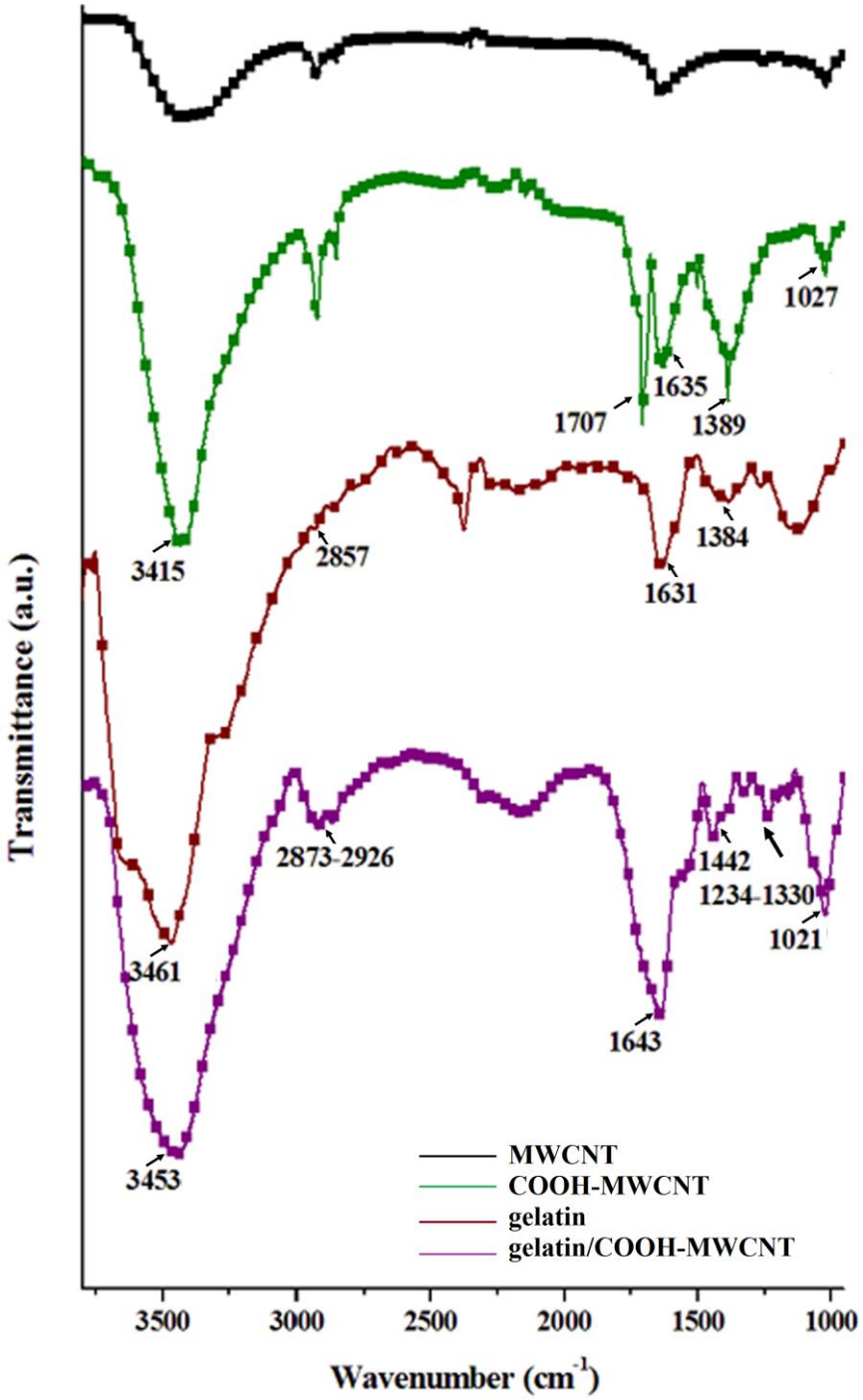

Fig. 5.5 FT-IR spectra of COOH-MWCNT, gelatin and nanocomposite gel

What's more, peaks at around 1643 cm^{-1} and 3453 cm^{-1} become broader and intense, which reveals the presence of COOH-MWCNTs. Some sort of chemical modification occurs in the structure of the polymer after the incorporation of COOH-MWCNT due

to which peaks becomes intense and shift towards higher wavenumber side. Moreover, additional peaks are found in the nanocomposite at 1234-1330 cm^{-1} and 1021 cm^{-1} which arises from the characteristic vibration of the C-O and O-H group of carboxyl functionalized MWCNT.

Table 5.1 Characteristic vibrational modes of COOH-MWCNT, gelatin and nanocomposite gel

Wavenumber (cm^{-1}): Characteristic bond		
COOH-MWCNT	**Gelatin**	**Gelatin/COOH-MWCNT**
1027: O-H bending		1021: O-H bending
1389: C-O stretching		1234-1330: C-O stretching
	1384:CH=N absorption (aldimine)	1442: CH=N absorption (aldimine)
1635: C=C stretching		
1707: C=O stretching (carboxyl)	1631: C=O stretching (amide)	1643: combination of C=O stretching of amide and carboxyl
	2851: C-H stretching	2873-2926: C-H stretching
3415: O-H stretching (carboxyl)	3461: N-H stretching (amide)	3453: combination of O-H (carboxyl) and N-H stretching (amide)

5.4.3 Optical analysis (UV-visible)

The optical absorption property of the gel electrolyte is carried out by UV-visible spectroscopic analysis [Fig. 5.6]. In the UV-visible spectrum of COOH-MWCNT, a characteristic peak is observed at 244 nm is due to the $\pi \rightarrow \pi^*$ transition of –COOH group.[35] In addition, a peak at around 288 nm which is due to the $\pi \rightarrow \pi^*$ transition of aldimine linkage of gelatin is observed.[25, 33] A similar peak with slight broadening is also appeared in the nanocomposite. It can be assigned to the chemical modification around the aldimine linkage in the presence of MWCNTs which causes the observed effect, which is in agreement with FT-IR analysis [Fig. 5.5]. In the nanocomposite, an enhancement in the optical absorbance occurs in the wavelength range longer than 400 nm. This can be attributed to the enhancement of surface electric charge of the oxides

in the nanocomposite gel with the incorporation of MWCNTs. Due to the presence of COOH-MWCNTs possible electronic transition occurs which is due to $\pi \rightarrow \pi^*$ transition of the functionalized nanotubes and $n \rightarrow \pi^*$ transition between the n-orbit of the oxygen species in the matrix.[36]

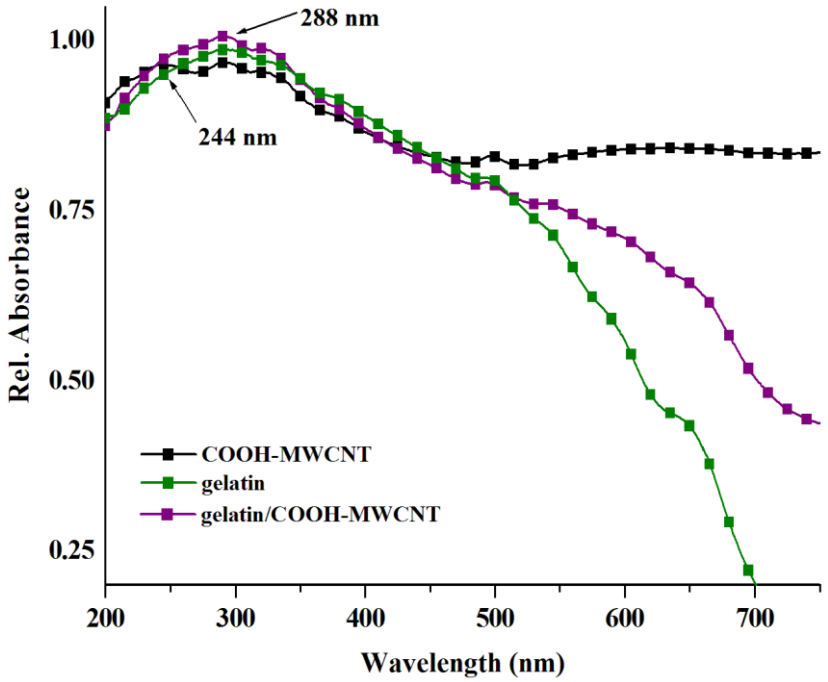

Fig. 5.6 UV-visible spectra of COOH-MWCNT, gelatin and nanocomposite gel

5.4.4 Electrochemical impedance spectroscopy (EIS)

To evaluate the interfacial charge transfer resistance of gelatin/COOH-MWCNT gel electrolytes in the DSSCs and also to study the effect of MWCNT concentration on device performance, EIS analysis of the devices has been performed. Devices are exposed under the simulated AM 1.5G 100 mW/cm^2 illumination. A commercially available ZnO is used to study the effect of COOH-MWCNT on the devices. Fig. 5.7 (b) shows the Nyquist plot of a set of gel electrolyte with various percentage of nanotube using the ZnO photoanode. Under exposure to light, the biased device shows a small arc in the high frequency range, which results from the capacitance resistance at the counter electrode/gel electrolyte interface (R_{ct1}), i.e., the charge transfer resistance at the Pt electrode/electrolyte interface.[25] Another larger arc occurs at low frequency range due to the presence of the charge transfer resistance (R_{ct2}) at the

electrolyte/ZnO electrode interface.[25] In each graph an extended tail is observed which may be due to the Warburg diffusion process of the I^-/I_3^- redox couple.[23] The gel

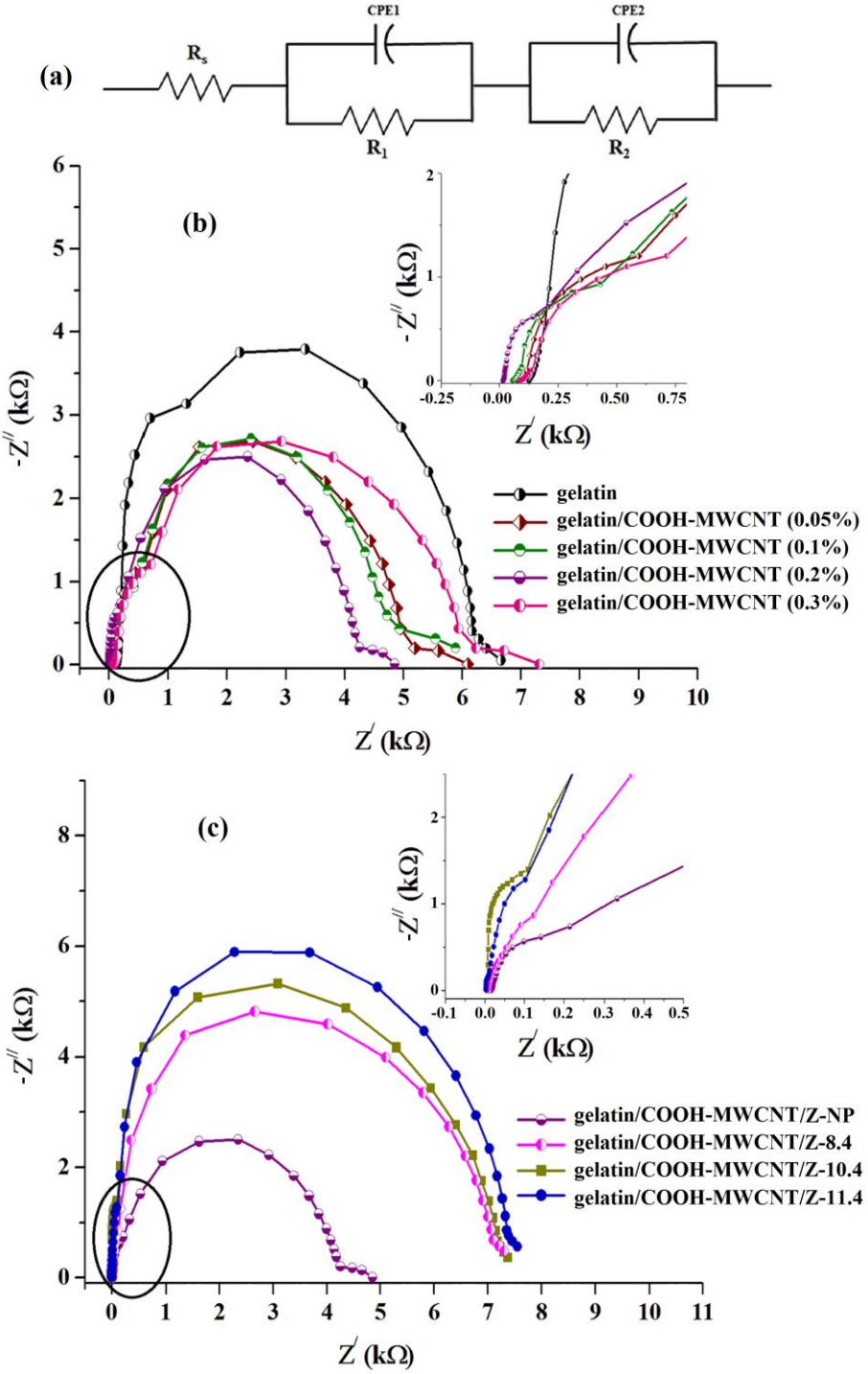

Fig. 5.7 (a) equivalent circuit diagram for the device; EIS analysis spectra of the gel electrolyte under illumination: (b) with different concentration of COOH-MWCNT, (c) with different aspect ratio of ZnO nanorods. Insets show the expansion of the respective areas indicated by the circles. *NP-commercial ZnO nanoparticle

electrolyte is also associated with a series resistance (R_s) which is mentioned in Table 5.2. From the table it is observed that in presence of carbon nanotubes both R_{ct1} and R_{ct2} for the nanocomposite gel electrolyte become smaller than their pristine counterpart. MWCNTs provide increased interfacial contact between the electrolyte and electrode arises from the large active surface area of the electrolyte. It causes increase in charge transfer process between Pt and ZnO electrodes and also migration of ions (I^-/I_3^-) in the electrolyte. Subsequently, resistance decreases in comparison to their pristine gel electrolyte.[23, 25] As we increase the concentration of carbon nanotubes upto 0.2%, the active surface area has a more pronounced effect on reduction of R_{ct1} and R_{ct2}. As a consequence of this the migration of ions and charge transfer process are improved to a large extent. In all the nanocomposite devices J_{sc} becomes significantly large, which is due to the rapid migration of ions and transport of electrons through different channel arises from the large interfacial contact between the electrolyte and ZnO layer [Fig. 5.10 (a)]. On the contrary, when we further increase the nanotube content, the charge transfer resistance starts increasing which arises due to the formation of solid networks in presence of excess nanotubes. This solid network hinders the transfer of electron from counter electrode to the electrolyte as the network is in contact with the counter electrode.[25] Consequently, device parameters are reduced after an optimum concentration (0.2%) of nanotubes. So, for an efficient device performance the optimum concentration of COOH-MWCNT is 0.2%.

To evaluate the effect of anisotropy of ZnO photoanode, we have also studied the EIS spectra for the synthesized ZnO nanorods (aspect ratio 8-20) using gelatin/COOH-MWCNT gel electrolyte with the optimum nanotube content of 0.2% [Fig. 5.7 (c)]. As previously seen, Fig. 5.7C also shows two distinct arcs: one at high frequency range which corresponds to the resistance related to charge transfer between the electrolyte and the counter electrode (R_{ct1}) and the other one represents the kinetics of the transport or recombination process occurring in the photoanode (R_{ct2}).[37] By changing the aspect ratio of photoanode, R_{ct1} remains almost same even though it is less than those using commercially available ZnO nano-powders, but R_{ct2} significantly increases with increase in the aspect ratio of the ZnO nanorods. R_{ct2} is increased in the sense that the ZnO nanorods act as the bridge which facilitates the collection and transport of

electrons at the interface of photoanode and the electrolyte. Consequently, the transport mechanism becomes faster. This reduces the electron recombination which increases the electron life time in the photoanode.[38] The transport and collection mechanism becomes more faster at larger nanorods which renders high recombination resistance as a consequence of which device parameters such as V_{oc}, J_{sc} and PCE become high [Table 5.4].

Table 5.2 Various parameters determined by EIS measurements for the nanocomposite gel

Device	R_s (kΩ)	R_{ct1} (kΩ)	$^{*}R_{ct2}$ (kΩ)	δ (Scm^{-1}) $x10^{-3}$
Gelatin	0.13	1.19	4.86	1.6
Gelatin/(0.05%)COOH-MWCNT	0.08	0.52	4.61	2.7
Gelatin/(0.1%)COOH-MWCNT	0.06	0.37	4.51	3.6
Gelatin/(0.2%)COOH-MWCNT	0.02	0.13	4.12	13
Gelatin/(0.3%)COOH-MWCNT	0.09	0.62	6.61	2.2
Gelatin/(0.2%)COOH-MWCNT/Z-8.4	0.01	0.11	6.99	18
Gelatin/(0.2%)COOH-MWCNT/Z-10.4	0.006	0.101	7.08	33
Gelatin/(0.2%)COOH-MWCNT/Z-11.4	0.002	0.100	7.25	100

$^{*}R_{ct2}$ has different significance in both sets of devices

5.4.5 Study of thermal properties (TGA, DSC)

The thermal stability of the gel with or without COOH-MWCNT is studied by TGA and DSC analysis in the temperature range 25-600 °C [Fig. 5.8 & 5.9]. Summary of the results are shown in Table 5.3. The nanocomposite gel electrolyte shows better thermal stability than their pristine polymer. For instance, major degradation starts in the temperature range 193-357 °C for the neat gelatin with the major degradation temperature (T_d) at 302 °C. Conversely, for all the nanocomposite gels, major degradation starts at remarkably higher temperature, in the range 233-397 °C. Upon heating a polymer, the free radicals are formed at the weak bonds and these radicals will transfer to the adjacent chains via inter-chain reactions. The incorporation of MWCNT into the polymer matrix reduces the mobility of the polymer chains which suppressed the chain transfer reactions. Thus, the degradation process is delayed and

decomposition starts comparatively at higher temperature.[25, 39] This imparts improved thermal stability in the nanocomposites. Moreover, MWCNT in the gelatin matrix has the role as a mass transport barrier towards the evolution of volatile products during thermal degradation and hence increases the overall thermal stability of the polymer.[25]

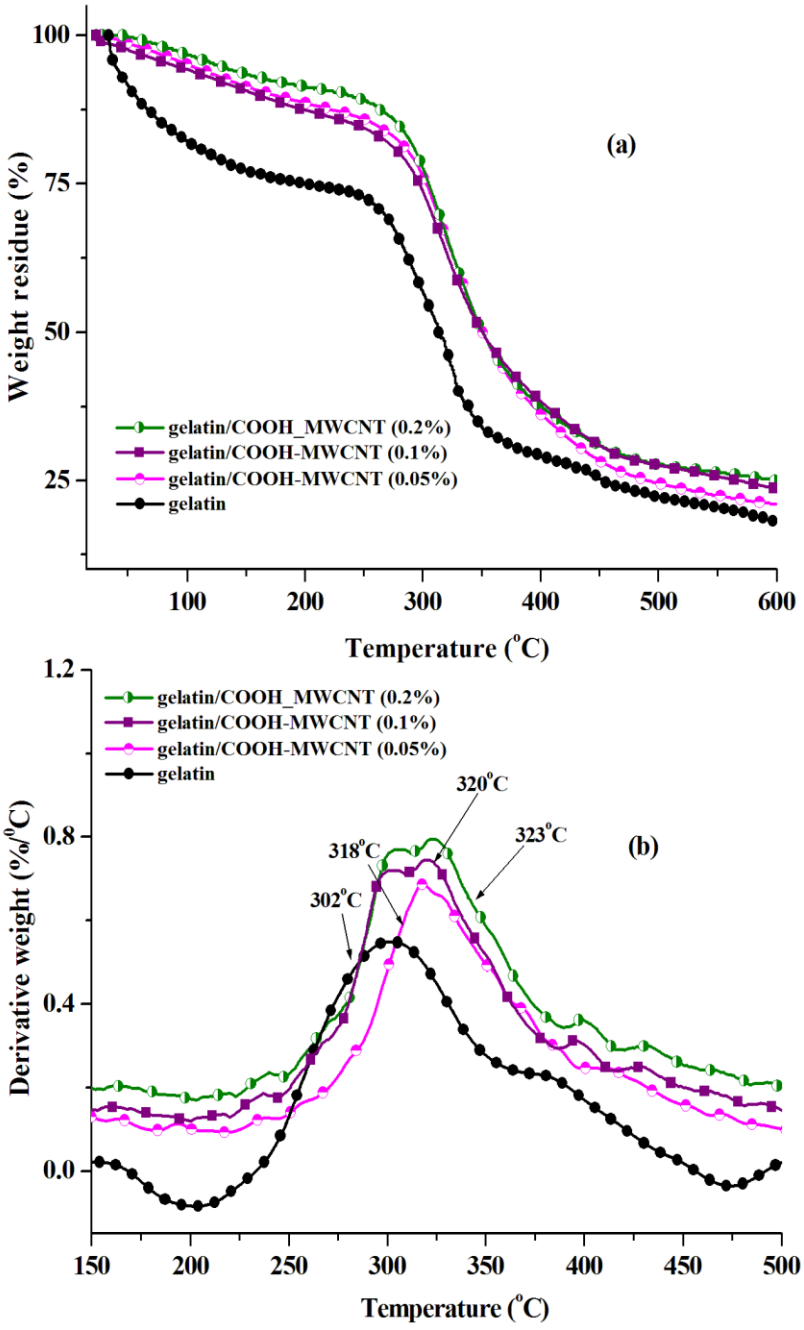

Fig. 5.8 (a) TGA and (b) DTG curves of gelatin and nanocomposite gel with different concentration of COOH-MWCNTs

Fig. 5.8 depicts that with an increase in the concentration of MWCNT upto an optimum concentration of 0.2%, T_d shifts to higher values. This observation is

qualitatively consistent with the DSC results [Fig. 5.9]. With increase in MWCNT content, the glass transition temperature (T_g) of the polymer increases which can be endorsed by the more reduced mobility of the polymer segments that promotes the delay of the degradation process.[25, 39] Again, an increase in the concentration of MWCNT leads to the enhancement in the mass transport barrier.

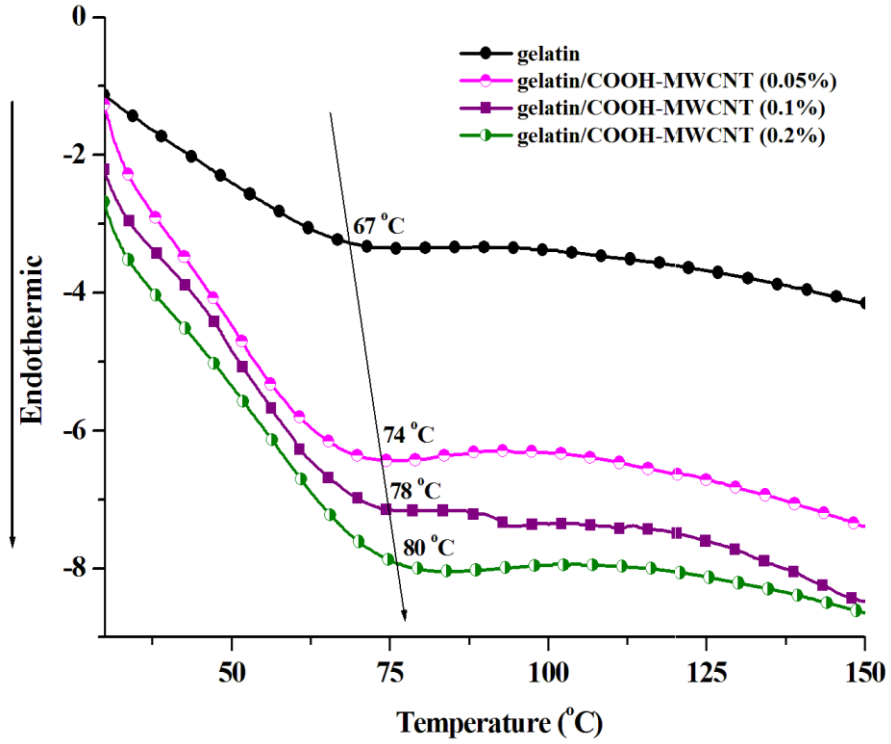

Fig. 5.9 DSC traces of gelatin and nanocomposite gel with different concentration of COOH-MWCNTs

Table 5.3 Thermal data from TGA and DSC

Sample particulate	Major degradation range (°C)	T_d (°C)	T_g (°C)
Gelatin	193-357	302	67
Gelatin/COOH-MWCNT (0.05%)	240-397	318	74
Gelatin/COOH-MWCNT (0.1%)	244-395	320	78
Gelatin/COOH-MWCNT (0.2%)	247-390	323	80

5.4.6 Evaluation of photovoltaic performance

To evaluate the effect of MWCNT concentration on photovoltaic performance of

DSSCs, initially we have studied the device performance using the commercially available ZnO nano powders [Fig. 5.10 (a)]. By changing the COOH-MWCNT content in the gel electrolyte, it is observed that at an optimum concentration of 0.2% COOH-MWCNT there is a significant increase in PCE of 0.21% [Table 5.4]. The conducting MWCNT offers a large interfacial contact between the electrolyte and electrode due to the large active surface area of the electrolyte. It causes an increase in charge transfer process between Pt and ZnO electrodes and migration of ions (I^-/I_3^-) in the electrolyte as well. Subsequently, a reduced resistance is observed in the nanocomposite electrolyte in comparison to pristine gelatin.[23, 25] Moreover, due to the presence of the COOH-MWCNTs, gelatin can properly be adsorbed onto the photoanode surface through Zn-O bonds. This can suppress the back electron transfer from the nanoparticle to the I_3^-. Consequently, the V_{oc} and J_{sc} of the device increase arising from the enhanced value of the quasi Fermi level of the conduction band electrons in the ZnO film.[25, 40] Further increase in nanotube content results in an adverse effect; i.e., decrease in device parameters. This may be due to the formation of a solid network in presence of excess nanotubes which hinders the electron transfer between the counter electrode and the electrolyte, as this network is in contact with the counter electrode.[25] From the above results, the optimum concentration of COOH-MWCNT in the gel electrolyte is found to be 0.2% for the best performance.

To study the effect of aspect ratio of ZnO nanorods, we have fabricated a set of DSSCs by using different aspect ratio ZnO photoanode with 0.2% concentration of COOH-MWCNT in the gel electrolyte [Fig. 5.10 (b)]. It is observed that the PCE of the devices increases almost 3 to 6-fold (0.69-1.35%) than the device fabricated by using the commercial ZnO nano-powders (0.07-0.21%). This may be due to the rod-like morphology of the ZnO nanocrystals that can act as the bridge to transport electrons between the electrodes. Thus, the nanorods facilitate the collection and transport of electrons in the photoanode thereby accelerating the charge transport mechanism. Subsequently, the electron recombination is reduced which increases the electron life time in the photoanode.[38]

With increase in aspect ratio the transport and collection mechanism becomes more faster which renders high recombination resistance and significantly high device

parameters such as V_{oc}, J_{sc} and PCE accordingly [Table 5.4]. For instance, for Z-8.4 the PCE is 0.69% while for Z-11.4 it is 1.35%. Moreover, it is be believed that high aspect ratio ZnO nanorods offer a larger surface area for dye molecules adsorption in

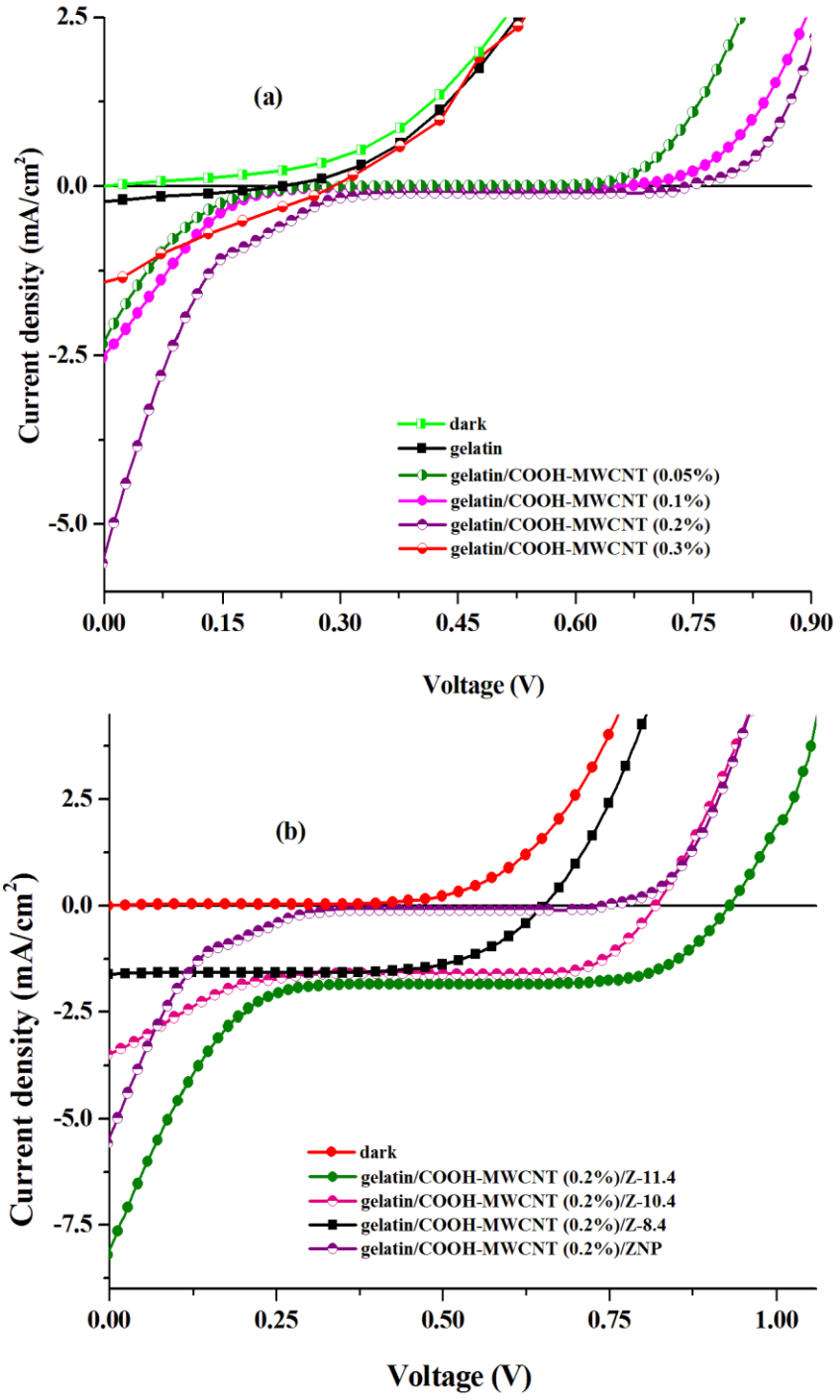

Fig. 5.10 J-V curves under illumination (a) with different concentration of COOH-MWCNTs, (b) with different aspect ratio ZnO nanorods as photoanodes. *The number denotes the pH of the medium

the photoanode thus leading to a strong light harvesting in the device. This imparts significantly high J_{sc} of 8.14 mA/cm^2 in the device.[41] Although, generally with an increase in aspect ratio the fill factor (FF) gradually decreases, it cannot affect on efficiency. The significantly high value of V_{oc} and J_{sc} dominate the effect of low FF. Hence, the PCE increases with aspect ratio in-spite of low FF.[42, 43]

Table 5.4 Photovoltaic characteristics of DSSCs

Device	V_{oc} (V)	J_{sc} (mA/cm^2)	FF	η (%)
Gelatin	0.23	0.23	0.29	0.02
Gelatin/(0.05%)COOH-MWCNT	0.36	2.3	0.09	0.07
Gelatin/(0.1%)COOH-MWCNT	0.66	2.51	0.06	0.10
Gelatin/(0.2%)COOH-MWCNT	0.74	5.53	0.05	0.21
Gelatin/(0.3%)COOH-MWCNT	0.30	1.43	0.21	0.09
Gelatin/(0.2%)COOH-MWCNT/Z-8.4	0.65	1.62	0.65	0.69
Gelatin/(0.2%)COOH-MWCNT/Z-10.4	0.82	3.48	0.37	1.06
Gelatin/(0.2%)COOH-MWCNT/Z-11.4	0.93	8.14	0.18	1.35

5.5 Conclusion

- We have prepared a set of DSSCs by using hydrothermally synthesized high aspect ratio ZnO nanorods as the photoanode and gelatin/MWCNT as the gel electrolyte.
- An optimum concentration of MWCNT (0.2%) in the gel electrolyte shows the best performance.
- As the aspect ratio of ZnO nanorods increases from 8 to 20, the PCE increases from 0.69% to 1.35% due to the rapid charge transport in the photoanode.
- ZnO nanorods offer an improved rate of collection and transport of electrons through the channels of the nanorods. It promotes the enhancement of device parameters.
- A large amount of dye molecules are absorbed in the photoanode thus leading to a strong light harvesting in the device. This offers a significantly high J_{sc} value.

- The overall result of this study suggests that anisotropic ZnO nanorod photoanode of aspect ratio 20 shows a maximum PCE of 1.35% in a quasi solid state DSSC at an optimum MWCNT concentration of 0.2% in the gel electrolyte.

References

1. Mehmood, U., et al. *Adv. Mater. Sci. Eng.* doi.org/10.1155/2014/974782, 2014.
2. Grätzel, M. *Inorg. Chem.* **44**, 6841-6851, 2005.
3. Martinson, A.B.F., et al. *Nano Lett.* **7**, 2183-2187, 2007.
4. Law, M., et al. *Nat. Mater.* **4**, 455-459, 2005.
5. Yoshida, T., et al. *J. Electrochem. Soc.* **150**, C608-C615, 2003.
6. Paulose, M., et al. *J. Phys. D: Appl. Phys.* **39**, 2498-2503, 2006.
7. Tyona, M.D., et al. *Adv. Nano Res.* **1**, 43-58, 2013.
8. Ku, C.H., et al. *Nanotechnology* **18**, 505706(1-9), 2007.
9. Lupan, O., et al. *J. Photochem. Photobiol. A: Chem.* **211**, 65-73, 2010.
10. Galoppini, E., et al. *J. Phys. Chem. B* **110**, 16159-16161, 2006.
11. Martinson, A.B.F., et al. *Phys. Chem. Chem. Phys.* **8**, 4655-4659, 2006.
12. Tubtimtae, A., & Lee, M.W. *Superlattice Microst.* **52**, 987-996, 2012.
13. Gao, X.D., Wang, C.L., Gan, X.Y., & Li, X.M. *Ordered Semiconductor Photoanode Films for Dye-Sensitized Solar Cells Based on Zinc Oxide-Titanium Oxide Hybrid Nanostructures*, *Nanostructures* Institute of Ceramics, P.R. China.
14. Du Pasquier, A., et al. *Appl. Phys. Lett.* **89**, 253513(1-3), 2006.
15. Lin, L.Y., et al. *Electrochim. Acta* **88**, 421-428, 2013.
16. Liu, H., et al. *Plos One* **10** (9), 1-17, 2015.
17. Zhu, S., et al. *Ceram. Int.* **40** (8), 11663-11670, 2014.
18. Zheng, Y.Z., et al. *Chem. Commun.* **47**, 11519-11521, 2011.
19. Lee, T.H., et al. *Nanoscale Res. Lett.* **6**, 1-8, 2011.
20. Akhtar, M.S., et al. *Electrochim. Acta* **55**, 2418-2423, 2010.
21. Arvanitoyannis, I.S. *Formation and properties of collagen and gelatin films and coatings* in *Protein-Based Films and Coatings*, A. Gennadios, eds., CRC Press, Boca Raton, 2002, 275-304.
22. Gennadios, A., McHugh, T.H., Weller, C.L., & Krochta, J.M. *Edible coating and films based on proteins* in *Edible Coatings and to Improve Food Quality*, J.M. Krochta, E.A. Baldwin, and M.O. Nisperos-Carriedo, eds. Technomic, Chicago, 1994, 201-277.
23. Nath, B.C., et al. *Electrochim. Acta* **146**, pp. 106-111, 2014.

24. Kim, S.L., et al. *J Appl. Electrochem.* **36**, 1433-1439, 2006.
25. Sharma, S., et al. *IEEE J. Photovolt.* **5**, 1665-1673, 2015.
26. Sharma, S., et al. *J. Polym. Mater.* **32**, 179-193, 2015.
27. Pokhrel, B., et al. *J. Electron. Mater.* **40** (2), 149-156, 2011.
28. Pradip, K., & Choudhury, A. *Sensor. Actuat. B-Chem.* **183**, 25-33, 2013.
29. Mishra, S.K., et al. *Appl. Phys. A* **115**, 1193-1203, 2014.
30. Jothi, N.S.N., et al. *Arch. Appl. Sci. Res.* **4**, 1698-1704, 2012.
31. Al-Harbi, L.M., et al. *Mod. Appl. Sci.* **5**, 87-91, 2011.
32. Cunha, C., et al. *Nanotechnology* **23**, 465102(1-10), 2012.
33. Nguyen, T.H., & Lee, B.T. *J. Biomed. Sci. Eng.* **3**, 1117-1124, 2010.
34. Narbat, M.K., et al. *Iran. Biomed. J.* **10**, 215-223, 2006.
35. Deborah, M., et al. *Spectrochim. Acta Part A* **139**, 138-144, 2015.
36. Dai, K., et al. *Nanotechnology* **20**, 125603(1-6), 2009.
37. Sima, M., et al. *Dig. J. Nanomater. Bios.* **8**, 757-763, 2013.
38. Lee, K.M., et al. *Sol. Energy Mater. Sol. Cells* **92**, 1628-1633, 2008.
39. Gogoi, P., et al. *J. Appl. Polym. Sci.* **132**, 41490(1-9), 2015.
40. Shalan, A.E., et al. *RSC Adv.* **5**, 103095-103104, 2015.
41. Wang, H., et al. *Beilstein J. Nanotechnol.* **3**, 378-387, 2012.
42. Cheema, H., et al. *Phys. Chem. Chem. Phys.* **17**, 2750-2756, 2015.
43. Chan, Y.F., et al. *J. Mater. Sci.* **48**, 5261-5272, 2013.